Journal of Power Sources 195 (2010) 8275–8279

Contents lists available at ScienceDirect

Journal of Power Sources

journal homepage: www.elsevier.com/locate/jpowsour

High rate-induced structural changes in thin-film lithium batteries on flexible substrate

Seung-Wan Song[a,*], Hyun Choi[a], Ho Young Park[b], Gi Back Park[b], Ki Chang Lee[b], Ha-Jin Lee[c]

[a] Dept. of Fine Chemical Engineering & Applied Chemistry, Chungnam National University, 220 Gung, Yuseong, Daejeon 305-764, South Korea
[b] Microcell Center, GS Nanotech Co., Ltd., Seoul 134-848, South Korea
[c] Korean Basic Science Institute, Jeonju 561-756, South Korea

ARTICLE INFO

Article history:
Received 24 May 2010
Received in revised form 18 June 2010
Accepted 28 June 2010
Available online 13 July 2010

Keywords:
High-rate capability
All-solid-state
Thin-film lithium battery
Structure
Multilayered encapsulation

ABSTRACT

An investigation is made of the high-rate capability (up to 10 C) of all-solid-state thin-film lithium batteries that comprise of Li/LiPON/$LiCoO_2$ on a flexible substrate, as well as of the effect of high-rate cycling on the structure of these batteries. Raman spectroscopic analysis results reveal that an increase in the rate promotes film orientation of the $LiCoO_2$ cathode with (1 0 1)/(1 0 4) planes and limited lithium intercalation and deintercalation within the layered hexagonal structure without a phase transition to monoclinic. Although with high-rate cycling the $LiCoO_2$ columnar grains tend to aggregate and lose grain orientation, as observed by scanning electron microscopic imaging, the film morphology is efficiently preserved when there is exterior multilayered encapsulation on thin-film batteries. Encapsulated thin-film batteries at 10 C show excellent capacity retention of 95% over 800 cycles, delivering > 22 $\mu Ah\,cm^{-2}\,\mu m^{-1}$. The data contribute to a basic understanding of the structure–rate performance relationship of all-solid-state battery systems.

1. Introduction

All-solid-state thin-film lithium batteries based on glassy lithium phosphorous oxynitride (LiPON) solid electrolytes [1,2] are being widely used as micropower sources in various electronic devices that range from information technology (e.g., smart cards, radio frequency identification (RFID) tags, e-paper, real-time clocks (RTCs), and memory backups) to bio-technology (e.g., drug delivery patches and medical implants) to ubiquitous sensing networks. Next-generation electronic devices require high-rate capability of thin-film lithium batteries for fast charging. It is generally recognized that thin-film batteries may exhibit poor rate capability because of the low ionic conductivity of solid electrolytes. The ionic conductivity of the LiPON film is three orders lower ($1.5 \times 10^{-6}\,S\,cm^{-1}$) [3–8] than that of conventional liquid electrolytes. It has been suggested, however, that the current density crosses in thin-film batteries is mainly limited by the resistance at the cathode|LiPON interface and lithium-ion diffusion in the cathode [4,9]. Studies on thin-film batteries that consist of sulfide-based solid electrolytes have found that the rate is influenced more by the cathode|electrolyte interfacial resistance than by the ionic conductivity of the solid electrolyte [10,11]. Thus, strong interfacial contact between the battery components could be a key factor in reducing the total resistance in the high-rate operation of a thin-film battery.

The authors have successfully manufactured flexible thin-film batteries of Li/LiPON/$LiCoO_2$ on a flexible mica substrate, which promotes interfacial contacts, by means of sequential sputtering coupled with rapid thermal annealing (RTA) technology [3–8]. The flexible thin-film batteries are easily shaped, sized and stacked at the required site and permit challenges with their free arrangement in-series or parallel to meet the required specific energy of electronic devices. Raman spectroscopy and scanning electron microscopy (SEM) were used to probe the structural changes that occur in the thin-film batteries with cycling [7,8]. Raman measurements using a laser beam with a submicron spot size that focuses on the required cross-section of the given thin-film battery seems adequate for precise characterization of the film structure of the $LiCoO_2$ cathode [7,8]. Structural investigation of thin-film battery components with high-rate cycling should allow a basic understanding of the structural changes that are responsible for consequent capacity variation and the different behaviour of cathode films with solid electrolyte from the bulk material in liquid electrolytes. This would pave the way for the enhancement of the performance and lifetime of thin-film batteries for wider use in future electronics. Studies of the effect of high-rate cycling on the structure of thin-film batteries have yet to be reported.

This investigation evaluates the high-rate capability of thin-film lithium batteries of Li/LiPON/$LiCoO_2$ on flexible mica substrate,

* Corresponding author. Tel.: +82 42 821 7008; fax: +82 42 822 6637.
E-mail address: swsong@cnu.ac.kr (S.-W. Song).

0378-7753/$ – see front matter © 2010 Elsevier B.V. All rights reserved.
doi:10.1016/j.jpowsour.2010.06.113

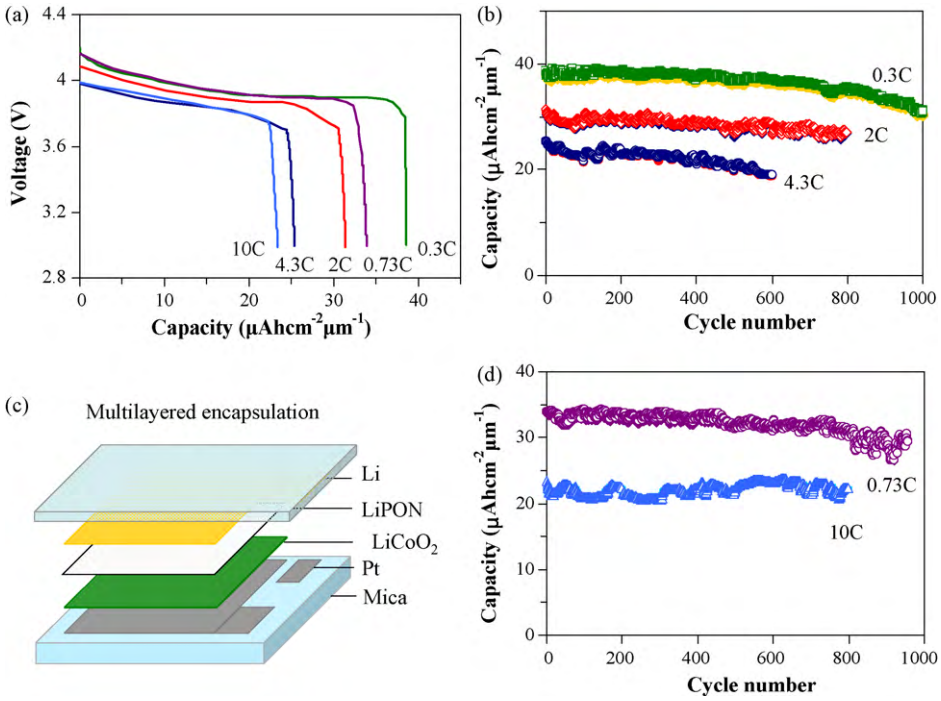

Fig. 1. (a) Initial discharge profiles of thin-film batteries of Li/LiPON/$LiCoO_2$ at a variable C-rate; (b) plots of capacity *vs.* cycle number at 0.3, 2 and 4.3 C without multilayered encapsulation; (c) a schematic of thin-film battery including multilayered encapsulation; (d) plots of capacities *vs.* cycle number at 0.73 and 10 C for thin-film batteries with multilayered encapsulation.

with mulilayered encapsulation. The rate-dependent structural changes that occur in the thin-film battery components are also examined.

2. Experimental

Thin-film lithium batteries that consisted of Li/LiPON/$LiCoO_2$ were fabricated using sequential sputtering and evaporation techniques [3–8]. A thin film of $LiCoO_2$ was first prepared using magnetron sputtering (power density 3.53 W cm^{-2} and 10 mTorr of Ar) on to a Pt/Cr current-collector film that was deposited on a flexible mica substrate of thickness 50 μm. The deposited $LiCoO_2$ film was heat-treated by RTA at 520 °C for 15 min. The thickness of the resulting $LiCoO_2$ films was 2.8–3.0 μm, as determined by field emission SEM (JEOL JSM-7000F) imaging at 5 kV. The film was found to be oriented with (1 0 1)/(1 0 4) planes (using X-ray diffraction and Raman spectroscopy). Then the LiPON film was deposited on the $LiCoO_2$ film by means of RF sputtering at 5 mTorr N_2 and 3.53 W cm^{-2} power using a Li_3PO_4 target. The thickness of the LiPON films was 1.45–1.5 μm, determined with field emission SEM imaging. The conductivity of the LiPON film was 1.5×10^{-6} S cm^{-1}, which was evaluated with impedance spectroscopy. The composition of LiPON was $Li_{2.64}P_{1.0}O_{2.81}N_{0.33}$, determined by inductively coupled plasma – atomic emission spectroscopy (ICP-AES) and elastic recoil detection – time of flight (ERD-TOF). This was followed by deposition of the Li anode via evaporation and of the Ni anode current-collector via sputtering, and by multilayered encapsulation. The total area and thickness of the thin-film batteries was 4 cm^2 (2 cm × 2 cm) and 10 μm, respectively. For multilayered encapsulation, the exterior of the thin-film batteries was alternately coated, layer by layer, 3–4 times with polymeric and oxide films using chemical vapour deposition and sputtering [12]. The encapsulation layers were transparent, so the shiny Li top layer was visible. The encapsulation allowed free handling of the thin-film batteries in air without the risk of atmospheric contamination or destruction.

The rate capability of the thin-film batteries was evaluated by cycling at constant current densities of 42 μA cm^{-2} (0.3 C) to 825 μA cm^{-2} (10 C) between 3.0 and 4.2 V *vs.* Li after the formation cycle at 0.3 C, using a multichannel cycler (Won-A Tech). The cycling was ended at a discharge voltage of 3.0 V, either when the capacity retention was <73% or when the cycle number was about 800–900. All electrochemical experiments were conducted in the Ar-filled glove box (MOTek) with individual water and oxygen contents of 1 ppm. Changes in the film morphology and microstructure on the battery cross-section with cycling were examined using *ex situ* field emission SEM and Raman spectroscopy, respectively. The Raman spectral measurement was conducted using a closed cell to avoid atmospheric contamination, and the cross-section (bulk) of the thin-film batteries was placed below a glass window in the glove-box. The spectra were recorded with a Raman microscope (Nanofinder 30, Tokyo Instrument Co.), using the 632 nm line of a He–Ne laser at 1 mW. Backscattering optics geometry with a double-notch filter and a standard charge-coupled device (CCD) detector were used to collect, process and analyze the Raman signal. The size of the laser beam at the sample was <200 nm.

3. Results and discussion

The voltage profiles of thin-film batteries during their initial discharge in the region of 3.0–4.2 V at 0.3–10 C are presented in Fig. 1a. The initial discharge capacity at 0.3 C is 39 μAh cm^{-2} $μm^{-1}$, whereas at 10 C it is reduced to 23 μAh cm^{-2} $μm^{-1}$, which is approximately 59% of the capacity at 0.3 C. It took just 5.9 min to charge the thin-film battery at 10 C.

The capacities of the thin-film batteries obtained at different C-rates are given in Fig. 1b and d. The capacities were calculated based on the thickness of the $LiCoO_2$ film, which was obtained from the SEM cross-section images. Fig. 1b shows that at 0.3 C, the thin-film battery retains 73% of its initial discharge capacity throughout 1040 cycles. With an increase in the C-rate to 2 C and 4.3 C, slight capacity fading occurs before the 100th cycle. With cycling at 4.3 C, the

capacity retention drops to 75% before the 600th cycle. High-rate capacity retention dramatically improves, however, when there is multilayered encapsulation on the exterior of the thin-film batteries, as displayed in Fig. 1c. With multilayered encapsulation, the thin-film battery at 0.73 C, in Fig. 1d, shows a greater capacity retention of 86% until the 960th cycle. The capacity retention improves significantly at 10 C to 95%, and delivers > 22 $\mu Ah\,cm^{-2}\,\mu m^{-1}$ over 800 cycles. This reveals that multilayered encapsulation is effective in obtaining high-rate performance. The cycling efficiency is higher than 99% for all the thin-film batteries, regardless of the C-rate. Considering that thin-film batteries are composed of film components, all of which are a few microns thick, and in particular the Li metal anode film, which is very sensitive to humidity and oxygen even at the level of a few ppm, encapsulation appears to provide protection from atmospheric contamination which can degrade their microstructure and performance. In the absence of multilayered encapsulation, thin-film batteries after cycling darkened slightly, regardless of the C-rate; whereas with multilayered encapsulation, the shiny top of the Li metal layer is still seen even after 800 cycles at 10 C. This supports the efficient role of multilayered encapsulation in protecting thin-film batteries. It is evident that atmospheric contamination of thin-film batteries even at a level of a few ppm is fatal and results in performance fading.

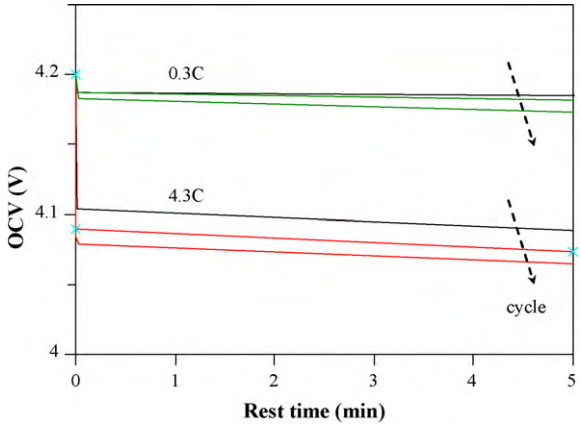

Fig. 2. Variation in OCV of thin-film batteries during rest following charge to 4.2 V at 0.3 and 4.3 C.

During the 5 min rest at the open-circuit voltage (OCV) after each charge and discharge process of the thin-film batteries, the OCV varies gradually with cycling, particularly at the higher C-rate. After the first charge to 4.2 V, the OCV decreases to 4.09 V at

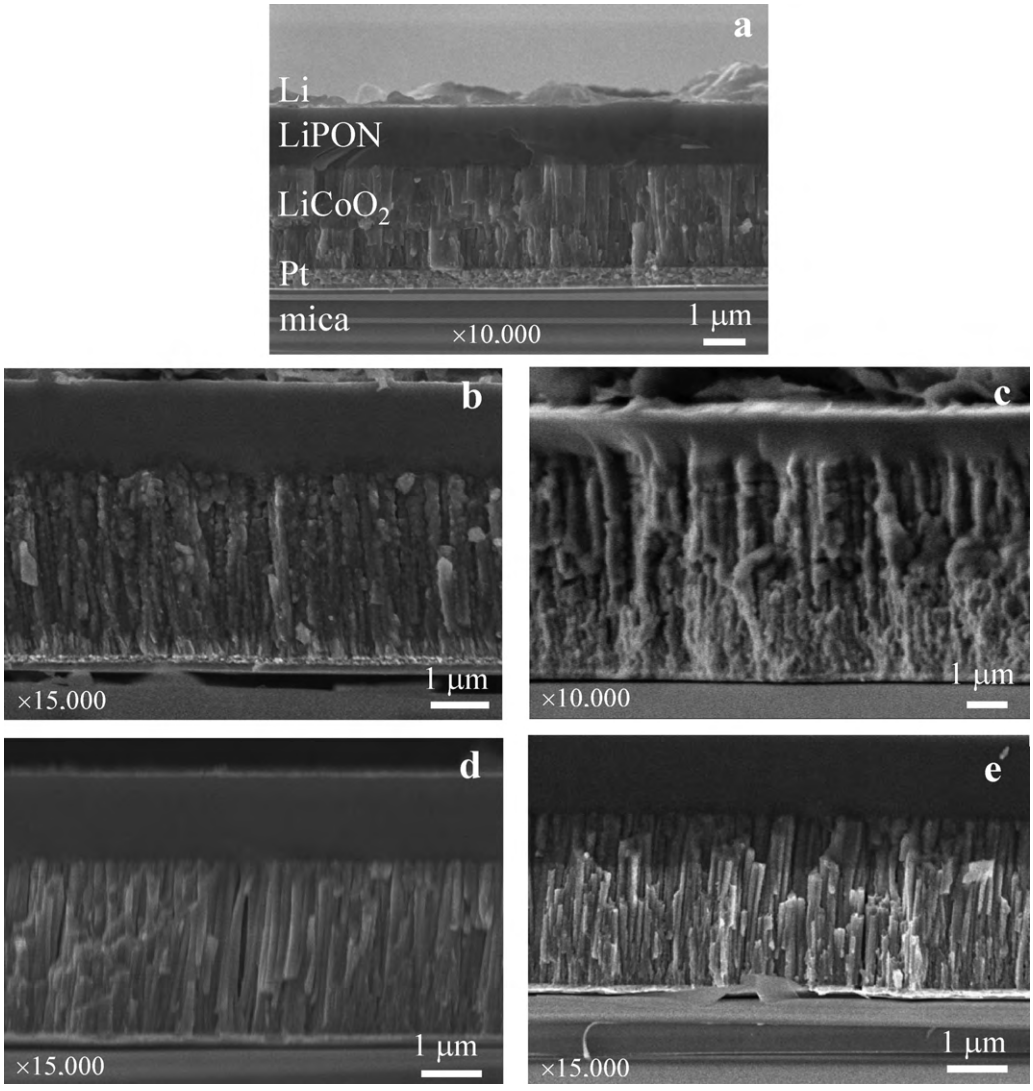

Fig. 3. Cross-sectional SEM images for thin-film batteries obtained after (a) formation cycle, and after cycling at (b) 2 C and (c) 4.3 C without multilayered encapsulation, and (d) 0.73 C and (e) 10 C with encapsulation.

4.3 C, whereas little change to 4.19 V is observed at 0.3 C as shown in Fig. 2. After the 600th cycle at 4.3 C, the OCV drops further to 4.06 V. Similar self-discharge behaviour is observed at 10 C. By contrast, the change in OCV after discharge to 3.0 V was independent of the C-rate, and increased to 3.90–3.91 V. By definition, charging the $LiCoO_2$ bulk cathode to 4.2 V in a liquid electrolyte, which corresponds to the de-intercalation of more than 0.55 lithium followed by significant *c*-axis expansion, gives rise to the formation of monoclinic (*C*2/*m*) phase with the approximate composition of $Li_{0.43}CoO_2$ due to the phase transition from hexagonal (*R*3-*m*) to monoclinic near 4.1 V [13]. In this context, the OCV of 4.06 V is attributed to the cathode film in the hexagonal phase. The *c*-axis expansion by lithium de-intercalation is found to be geometrically limited in thin-film batteries [7,8]. Also the diffusion kinetics of lithium ions can be limited, since current distribution at a high rate may not be homogeneous across thin-film batteries and high-rate cycling does not provide sufficient time to reach equilibrium in Li_xCoO_2. The limited *c*-axis expansion and current distribution with high-rate cycling of thin-film batteries appear to make the film maintain the hexagonal structure by self-discharge.

The change in morphology in the thin-film batteries due to high-rate cycling was monitored using *ex situ* SEM. The cross-sectional images of the thin-film batteries in Fig. 3 show the top of the battery layer by layer integration of Li, LiPON, $LiCoO_2$, and Pt/Cr films, and a mica substrate. The image in Fig. 3a reveals that, after the formation cycle, 110–200 nm wide columnar grains of the $LiCoO_2$ film are oriented as normal, and the interfacial contacts at $LiCoO_2$|Pt and LiPON|$LiCoO_2$ appear smooth. Such smooth interfaces achieved by RTA must be favourable for both long-term and high-rate cycling. With cycling at high rates in the absence of multilayered encapsulation, see Fig. 3b and c, reduced normal orientation of columnar grains normal and aggregation of the grains are observed. At 4.3 C (Fig. 3c), the aggregation of the columnar grains tends to be severe with loss of crystallinity. Near the interface of $LiCoO_2$|LiPON, the $LiCoO_2$ columnar grains show a horizontal line texture or cracks parallel to the substrate. Such horizontal texture, which is opposed to the columnar grains normal, may deleteriously affect the mechanical strength of the cathode film. Also shown in Fig. 3c is that the interfacial boundaries of $LiCoO_2$|Pt and $LiCoO_2$|LiPON become vague due to sticking and/or merging of the neighbouring layers. Thus, the thickness of the LiPON film appears significantly thinner than that of the other thin-film batteries, whereas the $LiCoO_2$ film appears thicker. The passage of a high current at 4.3 C across the thin-film batteries appears to have caused an electrochemical sintering effect on the $LiCoO_2$ and its interfaces, similar to long-term ageing of thin-film batteries [8,9]. A decline in the capacities at 4.3 C (Fig. 1b) should be related to this change in film morphology.

Multilayered encapsulation effectively enables preservation of film morphology. After cycling at 0.73 and 10 C (Fig. 3d and e) with multilayered encapsulation, not only the original morphology of the $LiCoO_2$ columnar grains but also the smooth interfaces between the layers are almost sustained. The morphology of all the battery component layers is maintained much better than without encapsulation (Fig. 3b and c), which is related to the observed excellent capacity retention in Fig. 1d. This emphasizes the necessity of multilayered encapsulation for protecting thin-film batteries from atmospheric degradation and obtaining a stable cycling performance.

A comparison of Raman spectra of $LiCoO_2$ films with C-rates is presented in Fig. 4. After the formation cycle (Fig. 4a), the film shows two bands at about 490 and 600 cm^{-1}, which are attributed to the vibration of oxygen atoms at the *ab* axis (E_g mode) and the *c* axis (A_{1g} mode) of the $LiCoO_2$ in the hexagonal layered structure [13], respectively. The relative intensity of the E_g band is similar to that of the A_{1g} band. This indicates that the bulk of the $LiCoO_2$ film has

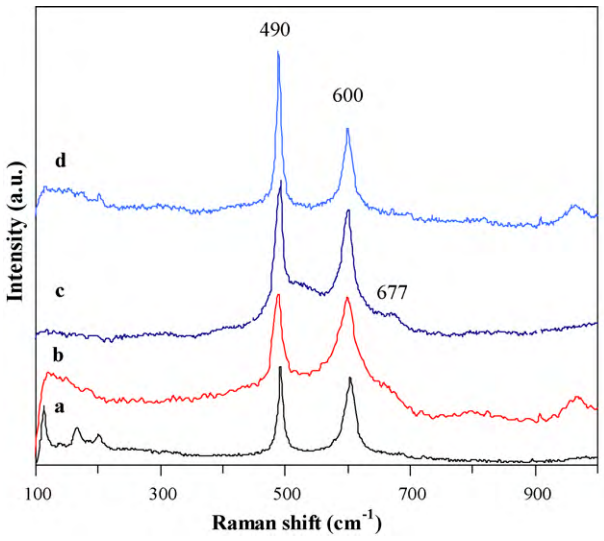

Fig. 4. Raman spectral comparison for cross-section of $LiCoO_2$ cathode film obtained after (a) formation cycle, and after cycling at (b) 0.73 C, (c) 4.3 C, and (d) 10 C.

a similar fraction of the (1 0 1)/(1 0 4)-oriented grains to the (0 0 3)-oriented grains [7,8,14]. After cycling at 0.73 and 4.3 C (Fig. 4b and c), a tiny shoulder appears near 677 cm^{-1} and is attributed to Co_3O_4 [15]. The presence of Co_3O_4 hinders lithium ion diffusion and lowers the electronic conductivity of the cathode and thereby, deleteriously influences the cycling performance. With cycling at 4.3 C, the E_g band is enhanced relative to the A_{1g} band, which corresponds to an increase in the fraction of the (1 0 1)/(1 0 4)-oriented grains. Further significant enhancement of the E_g band is observed after cycling at 10 C, as shown in Fig. 4d. Promoted film orientation with the (1 0 1)/(1 0 4) planes should be favoured for lithium ion transport and electron transfer kinetics, in particular, with high-rate cycling. Earlier reported results showed [16] that the strain energy of (1 0 1)/(1 0 4) planes in a $LiCoO_2$ film is much larger than that of other planes [16]. All-solid-state thin-film batteries are known to include stress and strain energy factors from the as-deposited film [14]. The increased strain energy from the increased fraction of the (1 0 1)/(1 0 4)-oriented grains in the cathode film can be compensated by aggregation of the columnar grains by lowering the surface energy, as shown in Fig. 3. Even with multilayered encapsulation, a thin-film battery cycled at 10 C tends to show aggregation of the $LiCoO_2$ columnar grains (Fig. 3e) near the interface with the Pt current collector layer. The passage of a high current during cycling appears to promote film orientation, but has an electrochemical sintering effect on film morphology, i.e., aggregation. Improved lithium transport kinetics due to the promoted film orientation of the hexagonal $LiCoO_2$ at 10 C and the preserved film morphology of the thin-film batteries due to multilayered encapsulation lead to excellent capacity retention of 95% over 800 cycles, as shown in Fig. 1d.

4. Conclusions

The high-rate capability of thin-film batteries up to 10 C and the importance of understanding of structure–rate performance relationship are demonstrated. With increasing C-rate, film orientation with (1 0 1)/(1 0 4) planes favoured for lithium transport kinetics is found to be enhanced in the $LiCoO_2$ cathode film, with a little loss of columnar grains normal and aggregation of grains. High-rate cycling also induces limited lithium transport within the hexagonal phases by self-discharge. Multilayered encapsulation allows the protection of thin-film batteries from atmospheric degradation

and the preservation of film morphology. Encapsulated thin-film batteries exhibit significantly improved capacity retention of 95% at 10 C over 800 cycles.

Acknowledgements

This work was supported by the Korea Energy Management Corporation under Contract No. 2006-E-EL02-P-01-3-010. Authors thank C.-C. Nguyen, Y.-S. Bae, J. Song and K.-H. Lee for their help with experiments.

References

[1] J.B. Bates, N.J. Dudney, G.R. Gruzalski, R.A. Zuhr, A. Choudhury, C.F. Luck, J.D. Robetson, Solid State Ionics 53–56 (1992) 647.
[2] X. Yu, J.B. Bates, G.E. Jellison Jr., F.X. Hart, J. Electrochem. Soc. 144 (1997) 524.
[3] H.Y. Park, S.R. Lee, Y.J. Lee, B.W. Cho, W.I. Cho, Mater. Chem. Phys. 93 (2005) 70.
[4] E. Jeong, C. Hong, Y. Tak, S.C. Nam, S. Cho, J. Power Sources 159 (2006) 223.
[5] H.Y. Park, S.C. Nam, Y.C. Lim, K.G. Choi, K.C. Lee, G.B. Park, S.R. Lee, H. Park Kim, S.B. Cho, J. Electroceram. 17 (2006) 1023.
[6] H.Y. Park, S.C. Nam, Y.C. Lim, K.G. Choi, K.C. Lee, G.B. Park, J.B. Kim, H.S. Park Kim, S.B. Cho, Electrochim. Acta 52 (2007) 2062.
[7] S.-W. Song, S.-W. Baek, H.Y. Park, Y.C. Lim, K.C. Lee, Electrochem. Solid State Lett. 11 (2008) A55.
[8] S.-W. Song, S.-J. Hong, H.Y. Park, Y.C. Lim, K.C. Lee, Electrochem. Solid State Lett. 12 (2009) A159.
[9] J.B. Bates, G.R. Gruzalski, N.J. Dudney, C.F. Luck, X. Yu, Solid State Ionics 70–71 (1994) 619.
[10] A. Hayashi, S. Hama, T. Minami, M. Tatsumisago, Electrochem. Commun. 5 (2003) 111.
[11] F. Mizuno, A. Hayashi, K. Tadanaga, M. Tatsumisago, Adv. Mater. 17 (2005) 918.
[12] Korean Patent No. 10-0832847.
[13] M. Inaba, Y. Iriyama, Z. Ogumi, Y. Todzuka, A. Tasaka, J. Raman Spectrosc. 28 (1997) 613.
[14] J.B. Bates, N.J. Dudney, B.J. Neudecker, F.X. Hart, H.P. Jun, S.A. Hackney, J. Electrochem. Soc. 147 (2000) 59.
[15] V.G. Hadjiev, M.N. Iliev, I.V. Vergilov, J. Phys. C: Solid State Phys. 21 (1988) L199.
[16] F.X. Hart, J.B. Bates, J. Appl. Phys. 83 (1998) 7560.